nature neuroscience

Negative functional MRI response correlates with decreases in neuronal activity in monkey visual area V1

Amir Shmuel, Mark Augath, Axel Oeltermann & Nikos K Logothetis

Most functional brain imaging studies use task-induced hemodynamic responses to infer underlying changes in neuronal activity. In addition to increases in cerebral blood flow and blood oxygenation level–dependent (BOLD) signals, sustained negative responses are pervasive in functional imaging. The origin of negative responses and their relationship to neural activity remain poorly understood. Through simultaneous functional magnetic resonance imaging and electrophysiological recording, we demonstrate a negative BOLD response (NBR) beyond the stimulated regions of visual cortex, associated with local decreases in neuronal activity below spontaneous activity, detected 7.15 ± 3.14 mm away from the closest positively responding region in V1. Trial-by-trial amplitude fluctuations revealed tight coupling between the NBR and neuronal activity decreases. The NBR was associated with comparable decreases in local field potentials and multiunit activity. Our findings indicate that a significant component of the NBR originates in neuronal activity decreases.

Functional brain imaging studies in humans rely on the measurement of cerebral blood flow (CBF)[1] or BOLD (refs. 2–5) signals. Recent studies have characterized the relationship between localized increases in neuronal activity and the corresponding increases in CBF (ref. 6) and BOLD (refs. 7–14), making it possible to interpret positive functional imaging responses in terms of neuronal activity. In addition to the commonly reported increases in these signals, sustained negative CBF (ref. 15) and BOLD (refs. 16,17) responses are pervasive in functional brain imaging studies. In contrast to the positive CBF and BOLD responses, the origin of the corresponding negative responses and their relationship to neural activity remain poorly understood.

To date, the origin of the NBR remains controversial. Some studies hypothesized a purely vascular origin (for example, 'vascular blood steal') for this phenomenon, suggesting that the NBR bears little direct relation to underlying neuronal activity[18–21]. Support for this proposal comes from an optical imaging study in the rat[22] that demonstrated an instance of low amplitude, negative hemodynamic response that did not correspond to observable changes in neuronal activity. A competing perspective suggests that the negative hemodynamic and BOLD responses reflect suppression of neuronal activity[15,18,19,23–26]. Some support for this view can be gleaned from a laser Doppler study that showed decreased cerebellar blood flow in response to reduced excitatory input to the rat cerebellum[27]. The same study, however, also reported that suppression of neuronal activity within the cerebral cortex was accompanied by a concomitant increase, rather than decrease, in CBF. A recent study in human cerebral cortex demonstrated prolonged NBR in early visual areas that was associated with decreases in CBF and with smaller decreases in oxygen consumption[16]. The findings from that study corroborate the contributions to the NBR of (i) a substantial component of decreases in neuronal activity (DiNA) and (ii) possibly, based on analysis of the time course of the NBR, a component of hemodynamic changes independent of the local changes in neuronal activity. To date, however, no direct measurements of neuronal activity have been performed within cerebral areas manifesting NBR.

The aim of the current study was to determine whether the NBR is associated with local changes in neuronal activity and, if so, to what extent the NBR can be accounted for by such changes. To address these questions, we applied electrical recordings simultaneously[7] with functional MRI (fMRI) in anesthetized macaque monkeys. The negative BOLD response beyond the stimulated regions of visual cerebral area V1 was found to be associated with—and coupled to—decreases in neuronal activity below spontaneous baseline activity. Our findings indicate that a substantial component of the negative BOLD response can be attributed to concomitant decreases in neuronal activity.

RESULTS

Association of NBR with decreases in neuronal activity

To characterize the neuronal correlates of the NBR in monkey V1, we used partial visual field stimulation in a protocol similar to one that elicits NBR in human visual cortex[16]. The recording electrode was located within visual area V1 (**Fig. 1**, green arrows). We used two stimuli, one of which overlapped with the aggregate receptive field (**Fig. 1**, green squares) of the neurons in the vicinity of the electrode. The nonoverlapping stimulus was either more peripheral or more central to the receptive field in the visual space. As expected, the overlapping stimulus elicited a positive BOLD response (PBR) near the electrode (**Fig. 1a**), whereas the nonoverlapping stimulus induced an

Max Planck Institute for Biological Cybernetics, Spemannstr. 38, 72076 Tuebingen, Germany. Correspondence and requests for materials should be addressed to A.S. (Amir.Shmuel@tuebingen.mpg.de) or N.K.L. (Nikos.Logothetis@tuebingen.mpg.de).

Received 28 February; accepted 6 March; published online 19 March 2006; doi:10.1038/nn1675

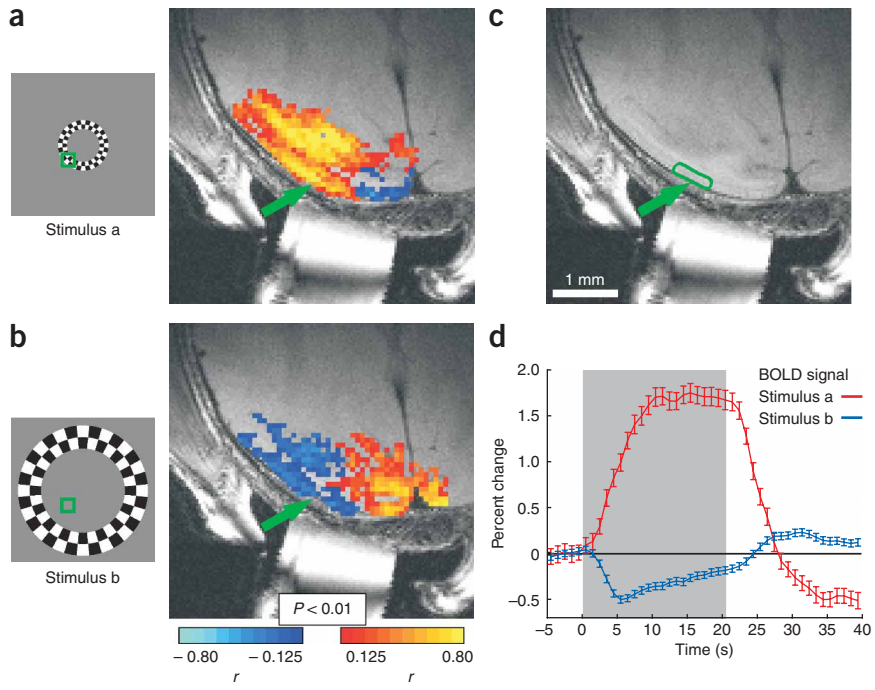

Figure 1 BOLD response to stimulation of part of the visual field. (**a**,**b**) Patterns of response to a central (3.5°–6.1°) and a peripheral (8.5°–14.7°) visual field stimulus. One oblique anatomical slice is shown, with the fMRI response superimposed on it. Green arrows, location of the recording electrode within visual area V1. Green squares, aggregate receptive field of the neurons in the vicinity of the electrode. The stimulus in **a** overlapped with the receptive field and induced a PBR in the vicinity of the electrode. The stimulus in **b** did not overlap with the receptive field and induced an NBR in that same vicinity. (**c**) The same anatomical slice as shown in **a** and **b**, with the ROI used to sample the BOLD signal superimposed in green. (**d**) Time course (mean ± s.e.m.) of the BOLD response sampled from the ROI around the electrode. The time courses presented here were averaged over all trials and sessions.

NBR in the same vicinity (**Fig. 1b**). A region of interest (ROI) encompassing the gray matter around the electrode was used to sample the BOLD signal (**Fig. 1c**). The mean NBR averaged over all data sets (**Fig. 1d**) was characterized by a transient, large-amplitude decrease in BOLD, followed by a gradual return towards the baseline. A poststimulus overshoot followed, which was approximately in phase with the poststimulus undershoot seen in the positive response.

To investigate changes in neuronal activity, we decomposed the broadband electrophysiological signal to obtain the spectrogram (power as a function of frequency and time). To first obtain an estimate of global neuronal activity, we averaged the fractional response over the whole range of frequencies (4–3,000 Hz). The time course of the global neural response associated with the positive BOLD response showed, as expected, that the stimulus that overlapped with the aggregate receptive field elicited increases in neuronal activity (**Fig. 2a**, time course averaged over all trials with the overlapping stimulus from all data sets). In contrast, the nonoverlapping stimulus induced DiNA beyond the stimulated regions of V1. We observed a transient, large-amplitude decrease in neuronal activity, followed by adaptation and a subsequent plateau of lower amplitude that was sustained below baseline over the entire stimulation period. The cessation of stimulation triggered an overshooting increase in neuronal activity, followed by a gradual decrease to the baseline level of activity.

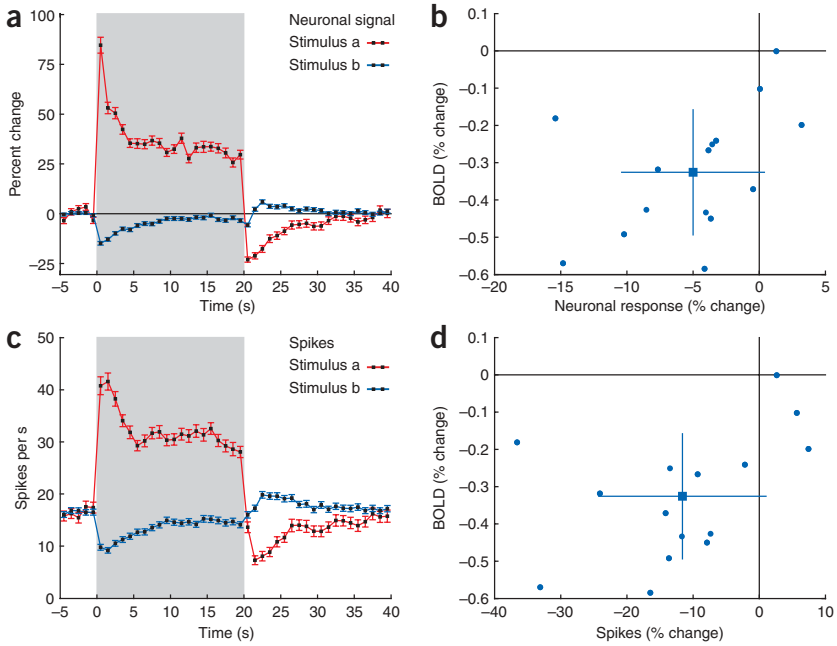

Figure 2 Neuronal and BOLD response to stimulation of part of the visual field. (**a**–**d**) Time course (mean ± s.e.m.) of (**a**) the fractional change in the comprehensive neuronal signal and (**c**) the action potential activity in response to stimuli that overlapped (red) or did not overlap (blue) the receptive field. The data in **a** and **c** were averaged over all trials and sessions. (**b**) Amplitude of the BOLD response as a function of the amplitude of the comprehensive neuronal response to the nonoverlapping stimulus. (**d**) Amplitude of the BOLD response as a function of amplitude of the action potential response to the nonoverlapping stimulus. In **b** and **d**, each data point represents the mean amplitude over one data set. The amplitudes of the responses were computed by averaging the time courses over the 12 s starting 2 s after the onset of the stimulus (for the neuronal response) and over the 12 s starting 2 s after the onset of the stimulus (for the BOLD response; see Methods). In **Supplementary Fig. 1**, the amplitudes are averaged over the entire epoch of stimulation (20 s). The blue square and bars depict the mean ± s.d. across all data sets.

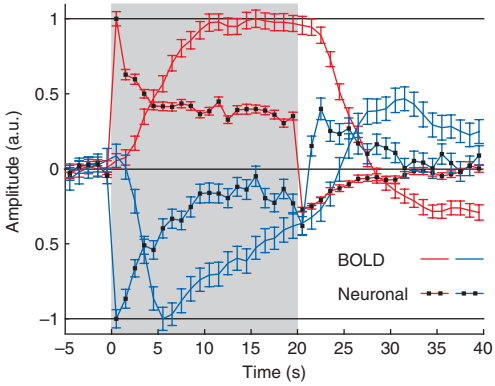

Figure 3 Dynamics of the NBR and decreases in neuronal activity. Normalized time courses of the BOLD and neuronal responses. The positive BOLD and neuronal responses were normalized by dividing each data point by the value of the corresponding peak response. The negative responses were normalized by dividing each data point by the absolute value of the negative peak response.

The mean BOLD response to the nonoverlapping stimulus, averaged over 15 data sets obtained from 7 monkeys, was negative (–0.33 ± 0.17%, mean ± s.d; **Fig. 2b**). In most of the experiments, the NBR was associated with DiNA. The corresponding mean neuronal response across data sets was negative (–5.00 ± 5.44%, $P < 0.005$, two-tailed *t*-test; **Fig. 2b**, **Supplementary Fig. 1** online). Note that in two experiments a low-amplitude NBR was associated with low-amplitude increases in neuronal activity (**Supplementary Fig. 2** online). To verify the overall DiNA, we used a second analysis method that did not rely on the decomposition of the neuronal signal according to frequency: namely, the detection and isolation of action potentials. We observed decreases in the average spiking activity relative to the spontaneous activity of neurons near the electrode (**Fig. 2c**), in response to stimulation outside their aggregate receptive field. The NBR was associated with decreases in the spiking activity of local neurons in most of the sessions (**Fig. 2d**), and the mean action potential response across sessions was negative (–11.61 ± 12.74%, $P < 0.005$, two-tailed *t*-test). Overall, the NBR was associated with DiNA.

Coupling of the NBR to decreases in neuronal activity

These findings suggest that DiNA may underlie the NBR. However, they do not rule out an alternative hypothesis: namely, that the DiNA are caused by reductions in CBF with a vascular origin. Decreases in CBF with a vascular origin (for example, vascular steal) could be the primary phenomenon, causing reduced oxygen availability within the NBR regions and thus instigating DiNA. NBRs are associated with decreases in CBF (refs. 16,28) and blood volume[20]. It is conceivable that the increase in arterial blood flow to the positively responding regions causes a decrease in blood flow to the NBR regions. If the decrease in CBF to the NBR regions was large, it could cause hypoxia, which in turn could prevent the neurons from maintaining their baseline neuronal activity. To rule out this possibility, we compared the dynamics of the NBR to those of the corresponding neuronal response (**Fig. 3**). The onset of the DiNA was immediate, similar to that of increases in neuronal activity. The onset and peak of the NBR lagged behind the onset and peak, respectively, of the DiNA. Therefore, the DiNA could not have been caused by hypoxia stemming from the decreases in CBF. Overall, the DiNA could not have been caused by decreases in CBF of a vascular origin.

One could further hypothesize that the NBR and the DiNA might co-occur at the same place and approximately the same time, without being related at all. It could be that the NBR is of purely vascular origin whereas the DiNA is of neuronal origin, and that the two phenomena

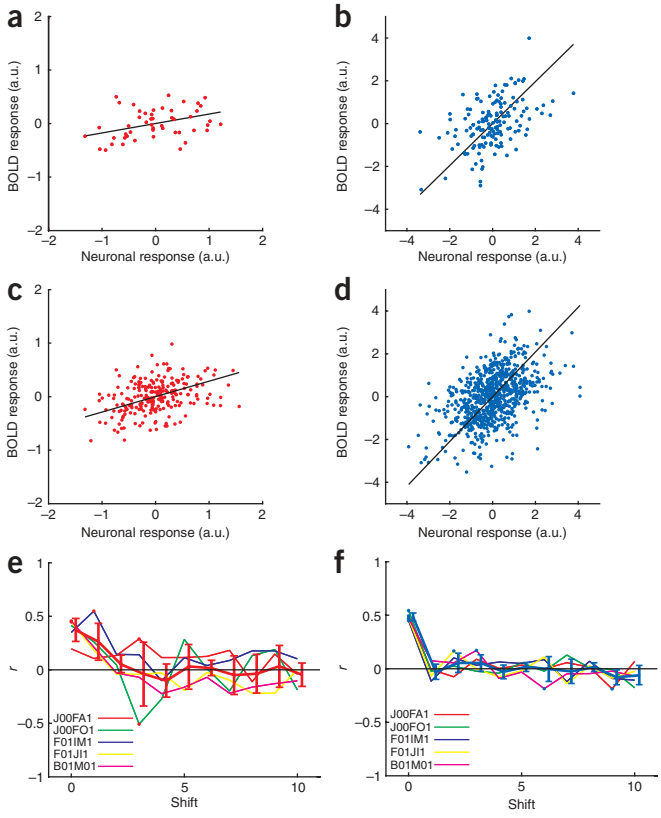

Figure 4 The negative BOLD response is correlated with decreases in neuronal activity. (**a**) Scatter plot of the amplitude of the PBR as a function of the increase in neuronal activity. The plot depicts the fluctuations in the PBRs and increases in neuronal activity in single trials relative to their mean responses over a single session (the mean responses were subtracted out; see Methods). Each dot depicts one trial with the stimulus that overlapped the receptive field. The dark line represents the result of regression using orthogonal fitting that considers measurement errors in both coordinates. Session F01.jI1. See also **Supplementary Figure 3**. (**b**) Scatter plot of the NBR as a function of the decrease in neuronal activity. The data are from trials with the stimulus that did not overlap the receptive field, from the same session as in **a**. Note that the nonoverlapping stimulus was presented in three times as many trials as the overlapping stimulus. (**c**) Scatter plot of the trial-by-trial amplitude of the PBR as a function of the increase in neuronal activity. The data are pooled from the five data sets with the largest DiNA. (**d**) Scatter plot of the NBR as a function of the decrease in neuronal activity. The data are pooled from the same five data sets as in **c**. (**e**) Correlation between the trial-by-trial PBR and the increase in neuronal activity. To test whether simultaneity is necessary for obtaining a positive correlation between the two responses, we shifted the trial-by-trial BOLD response forward in time relative to the trial-by-trial neuronal response. Correlation coefficients are presented as a function of the number of trials used to shift the trial-by-trial BOLD response. The red curve depicts the mean ± s.e.m. correlation averaged over the five data sets used in **c** and **d**. Each of the other colored curves represents one data set. A red dot stands for significant correlation obtained in a data set for the shift corresponding to the location of the dot. (**f**) Correlation between the trial-by-trial NBR and the decrease in neuronal activity. The data are from the same five data sets presented in **c**–**e**. The format is identical to that in **e**, except that a blue curve is used to present the mean ± s.e.m. over the data sets and blue dots mark significant correlations.

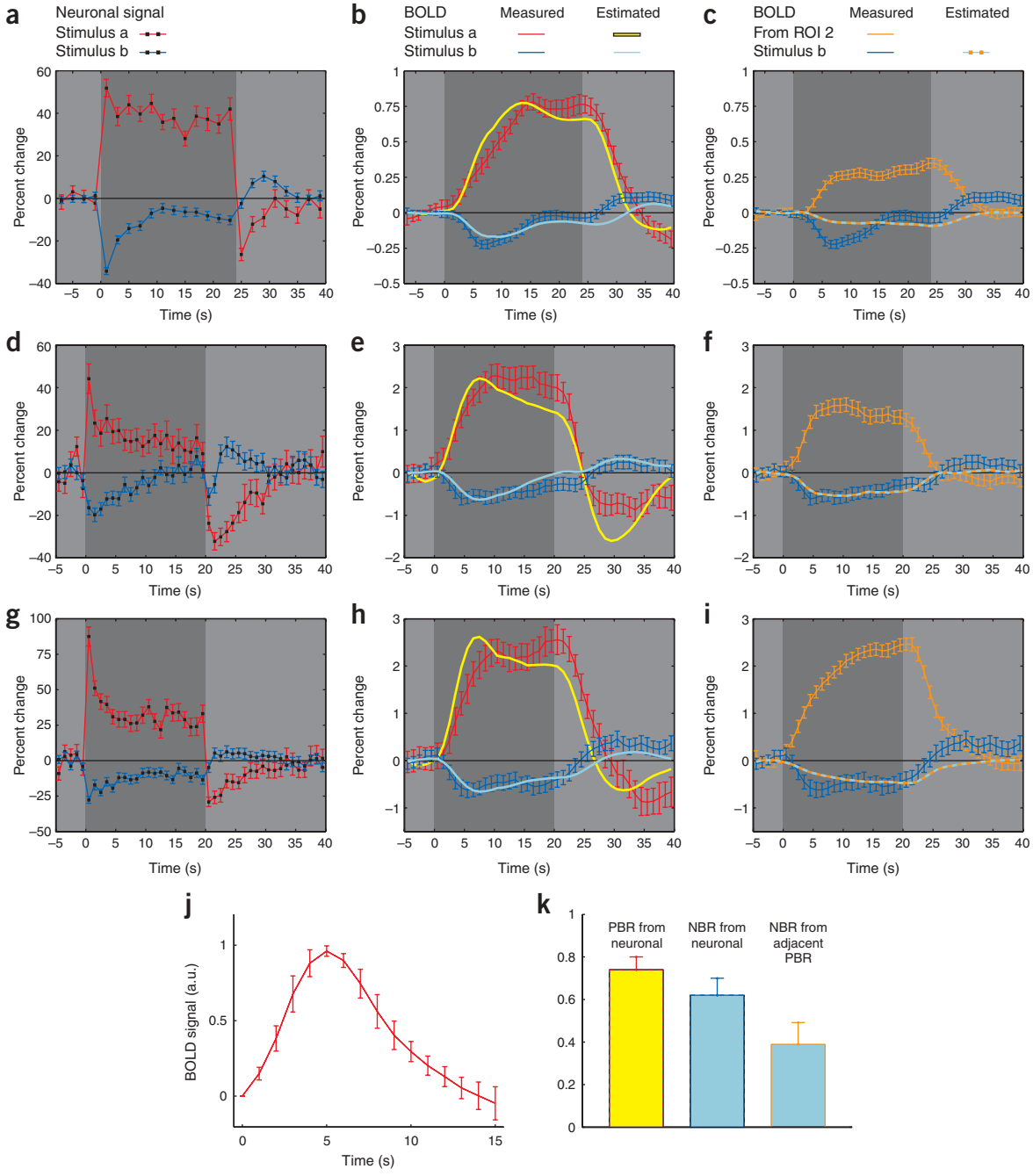

Figure 5 Prediction of the mean time course of the BOLD response from that of the mean neuronal response and adjacent BOLD response. (**a**–**j**) In **a**, **d** and **g**, mean neuronal response to the overlapping and nonoverlapping stimuli (mean fractional change in power averaged over the whole range of frequencies) obtained from sessions J00.fA1, F01.jI1 and B01.m01, respectively. In **b**,**e** and **h**, the corresponding predicted and measured BOLD responses obtained from the same sessions. To compute the predicted positive or negative response, the corresponding mean neuronal response presented in **a**,**d** and **g** was convolved with the impulse response in **j**. The result was then scaled using the scaling factor that would minimize the sum of squared differences between the predicted and measured response. In **c**, **f** and **i**, prediction of the time course of the negative BOLD response from that of the positive BOLD response from regions adjacent to the negative BOLD response from the same sessions. The curve in orange depicts the mean BOLD response from an ROI in V1, adjacent to the NBR. The positive response here was obtained simultaneously with the NBR that was observed in the vicinity of the electrode in response to the stimulus that did not overlap with the receptive field. To compute the predicted negative response (cyan-orange dashed line), the mean positive response (orange) was inverted and scaled to fit the measured response by minimizing the sum of squared differences between the predicted and measured response. (**j**) BOLD impulse response function. The cross-covariance of the BOLD and neuronal signals during spontaneous activity was computed as a function of positive lags in BOLD. The specific function obtained from each session was normalized to the range of 0 (for the first time point) to 1 (for the maximal value). The impulse response presented here is the mean ± s.e.m. over the five sessions with the largest DiNA. (**k**) Determination coefficient estimating the part of variance of the BOLD response that is accounted for by the different models. The first (yellow-red) and second (cyan-blue) bars to the left describe the estimation of PBR and NBR, respectively, from the comprehensive neuronal activity response. The third (cyan-orange) bar quantifies the estimation of NBR based on the time course of the PBR in adjacent regions. The data are the means ± s.e.m. averaged over all data sets that demonstrated DiNA.

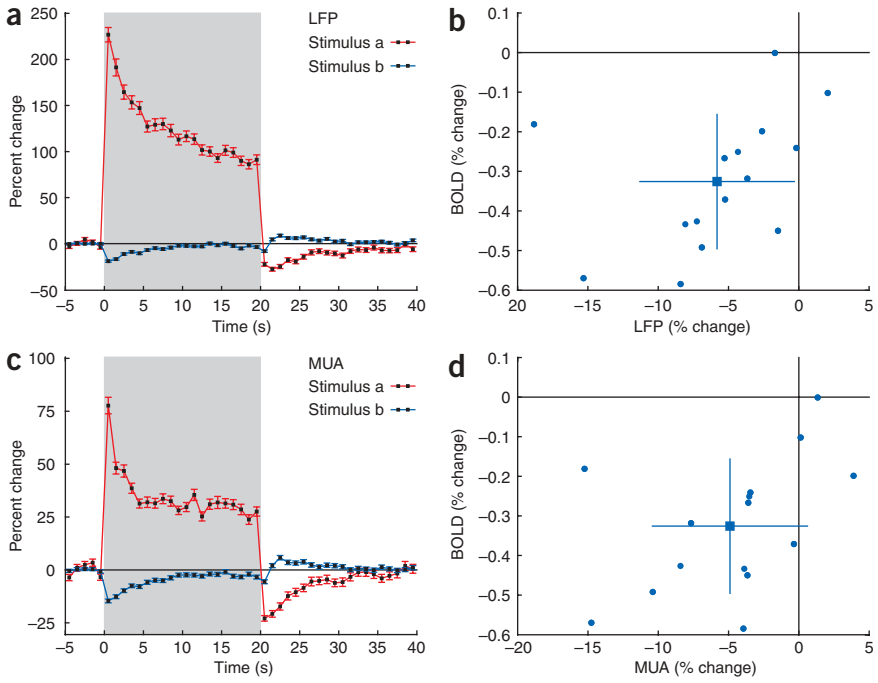

Figure 6 Neuronal and BOLD response to stimulation of part of the visual field: LFP and MUA. (**a**–**d**) Time course (mean ± s.e.m.) of (**a**) the LFP response and (**c**) the MUA response to stimuli that overlapped (red) or did not overlap (blue) the receptive field. The data in **a** and **c** were averaged over all trials and sessions. (**b**) Amplitude of the BOLD response as a function of the amplitude of the LFP response to the nonoverlapping stimulus. (**d**) Amplitude of the BOLD response as a function of amplitude of the MUA response to the nonoverlapping stimulus. In **b** and **d**, each data point represents the mean amplitude over one data set. The amplitude of responses were computed by averaging the time courses over the 12 s starting with the onset of the stimulus (for the neuronal response) and over the 12 s starting 2 s after the onset of the stimulus (for the BOLD response; see Methods). The blue square and bars depict the mean ± s.d. over all data sets.

are independent of each other. To establish whether the NBR and the DiNA are coupled, we analyzed the trial-by-trial fluctuations of the two different measured responses relative to their own mean responses across each session. The trial-by-trial amplitudes of the positive and negative BOLD response were correlated with those of the corresponding increases and decreases, respectively, in global neuronal activity (**Fig. 4a–b**; $r = 0.34$, $P < 2 \times 10^{-2}$; $r = 0.46$, $P < 10^{-8}$; regression using orthogonal fitting; data are from one data set; see also **Supplementary Fig. 3** online). Similarly, the trial-by-trial BOLD and neuronal responses pooled from the 5 data sets with the largest DiNA were correlated (**Fig. 4c–d**; $r = 0.35$, $P < 10^{-8}$ and $r = 0.46$, $P \approx 0$ for the positive and negative response, respectively).

To verify the coupling between the two responses, we checked whether the correlation between them depends on simultaneity (**Fig. 4e–f**). The mean (over the same five data sets) trial-by-trial correlation between the simultaneously measured NBR and DiNA was 0.485 ± 0.037 (**Fig. 4f**, shift = 0). To test the dependence on simultaneity, we repeated the correlation analysis with the same responses after shifting them with respect to each other so that the BOLD and neuronal responses being compared were not obtained simultaneously. The correlation between the DiNA and the shifted NBRs dropped to approximately 0 (**Fig. 4f**, shift ≥ 1). We thus concluded that the NBR was correlated with DiNA.

To further investigate the coupling between the NBR and the DiNA, we examined whether the time course of the BOLD response could be predicted from the time course of the neuronal response (**Fig. 5**). First we estimated the impulse response function (IRF) of the BOLD contrast by applying covariance analysis onto the time courses of the neural and hemodynamic signals. These time courses were recorded during epochs of spontaneous activity free of sensory stimulation at the beginning of each scan (**Fig. 5j**). We then convolved the mean positive and negative neuronal responses over one session (**Fig. 5a**) with the estimated IRF, to obtain the corresponding predicted BOLD responses (**Fig. 5b**). The predicted negative BOLD response captured the essential changes in the measured NBR (**Fig. 5b**). To test whether the NBR could

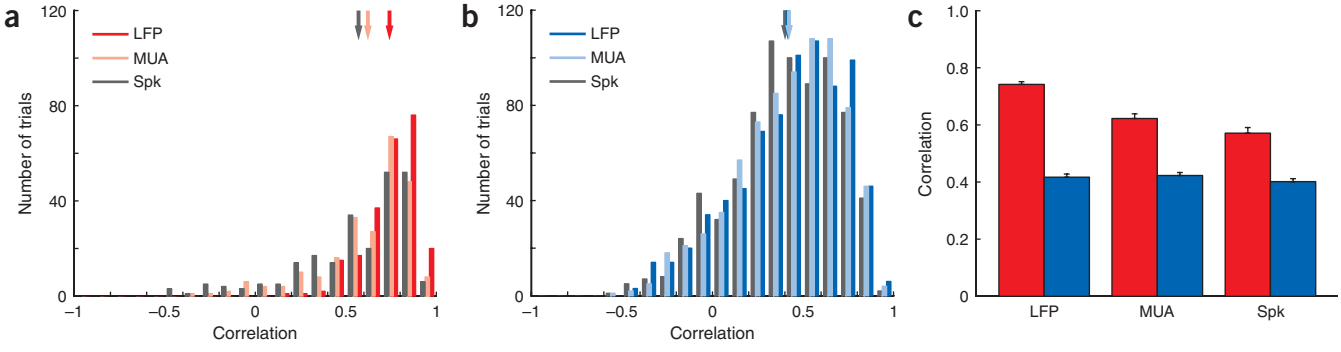

Figure 7 Trial-by-trial estimation of the time course of the negative BOLD response based on decreases in LFP, MUA and spiking activity. (**a**) Distributions of the correlation coefficients obtained by comparing the trial-by-trial time course of the measured PBR to that of the PBR predicted separately by the increase in LFP (red), MUA (pink) and spiking activity (gray). The arrows depict the means of the distributions. The data are pooled from the five data sets with the largest DiNA. (**b**) Distributions of the correlation coefficients obtained by comparing the time course of the measured NBR to that of the NBR predicted separately by the decrease in LFP (blue), MUA (cyan) and spiking activity (gray). The data are from trials with the stimulus that did not overlap the receptive field and are pooled from the same five data sets. (**c**) Mean ± s.e.m. of the correlation values presented in **a** for the PBR (red) and in **b** for the NBR (blue).

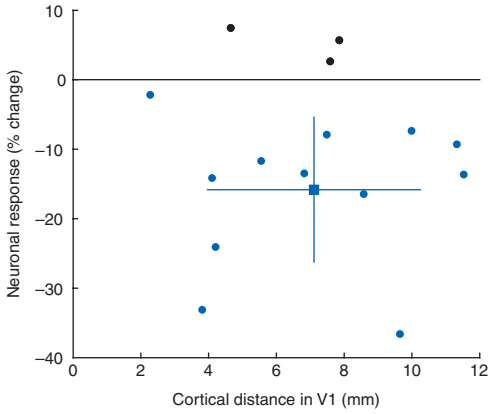

Figure 8 Distance between the closest positively responding region and the site where decreases in neuronal activity were detected. Neuronal response to the nonoverlapping stimulus is plotted as a function of the cortical distance from the electrode to the closest positively responding (PBR) region in V1. Each data point represents the mean amplitude of the action potential response to the nonoverlapping stimulus from one data set. The blue square and bars depict the mean ± s.d. over all experiments in which decreases in neuronal activity were detected (blue dots). The cortical distance was measured between the site where decreases in neuronal activity were encountered and the closest PBR parallel to the gray matter within the oblique/horizontal slice. Note that isoeccentricity rings retinotopically map to V1 as strips that run along the dorsoventral axis[47], approximately orthogonal to the curve along which the measurement was performed.

be predicted equally well by a model that assumed a purely vascular origin, we tested whether the time course of the NBR inversely mirrored that of the PBR from adjacent regions (**Fig. 5c**, **Supplementary Fig. 4** online). The predicted NBR based on the PBR from adjacent regions did not capture the changes in the measured NBR with the same fidelity as the predicted NBR based on the DiNA did. Similar results were obtained from two other monkeys (**Fig. 5d–f** and **Fig. 5g–i**, respectively). The time courses of the predicted NBRs based on the DiNA were highly correlated with—and accounted for most of the variance in—the corresponding measured time courses of NBR ($r^2 = 0.79$, 0.77 and 0.76; $p \approx 0$, 0 and 0; for **Fig. 5b**,**e** and **h**, respectively; linear regression). The mean determination coefficient averaged over all data sets that demonstrated DiNA was $r^2 = 0.74 \pm 0.06$ for the PBR and $r^2 = 0.62 \pm 0.08$ for the NBR (mean ± s.e.m.; **Fig. 5k**). The determination coefficient obtained for the NBR predicted by the vascular origin model averaged over the same data sets was $r^2 = 0.38 \pm 0.07$ (**Fig. 5k**), smaller than that obtained from the DiNA ($P < 0.02$, two-tailed pairwise *t*-test). We thus concluded that the time course of the NBR could be predicted from the local DiNA better than from the PBR in adjacent regions.

Association of NBR with decreases in LFP and MU activity

To investigate the coupling of the NBR to different bands of the neuronal signal, we examined the relationship of the NBR to changes in local field potentials (LFP) and multiunit activity (MUA; **Fig. 6**). The mean time courses (averaged over all trials and data sets) of the LFP and MUA responses (**Fig. 6a**,**c**) associated with the negative BOLD responses were similar to the corresponding time courses of the action potential and global neuronal responses (**Fig. 2**). The NBR was associated with decreases from baseline in both LFP (LFP response averaged over data sets: –5.81 ± 5.49%, mean ± s.d., $P < 0.005$, two-tailed *t*-test; **Fig. 6b**) and MUA (4.90 ± 5.51%, $P < 0.005$; **Fig. 6d**). The relative decreases in action potentials (**Fig. 2d**) were larger than the corresponding decreases in LFP and MUA ($P < 0.02$ and $P < 0.01$, $n = 15$, two-tailed paired *t*-test). The decreases in LFP were small relative to the increases in LFP associated with the PBR, but were comparable to the decreases in MUA associated with the NBR. To test whether the NBR was differentially coupled to these decreases in LFP, MUA and spiking activity, we compared the trial-by-trial time course of BOLD response predicted by these types of neuronal activity to the measured time course of BOLD response. We obtained the distribution of correlation coefficients (**Fig. 7**) by comparing the trial-by-trial measured BOLD time course to the BOLD time course predicted by convolving the time course of LFP, MUA and spikes with the estimated IRF (**Fig. 5j**). The data were pooled from the five data sets with the largest DiNA. As expected[7], the time course of the PBR was correlated with that of the increases in LFP, MUA and spiking activity (**Fig. 7a**,**c**; $r_{LFP} = 0.742 \pm 0.009$; $r_{MUA} = 0.622 \pm 0.017$; $r_{SPK} = 0.571 \pm 0.020$; mean ± s.e.m.; $n = 235$ trials). Similarly, the time course of the NBR was correlated with that of the decreases in these three types of neuronal activity (**Fig. 7b**,**c**; $r_{LFP} = 0.417 \pm 0.011$; $r_{MUA} = 0.423 \pm 0.010$; $r_{SPK} = 0.401 \pm 0.010$; $n = 762$ trials). The LFP response gave a better estimate of the PBR than the MUA or the action potential response did (mean r_{LFP} > mean r_{MUA}, $P < 9.0 \times 10^{-10}$; mean r_{LFP} > mean r_{SPK}, $P < 6.5 \times 10^{-14}$; two tailed *t*-tests), supporting previous reports of a closer coupling of PBR to LFP (ref. 7). The estimate of NBR based on LFP was not significantly different than the corresponding estimates based on MUA and action potentials ($P = 0.67$ and $P = 0.30$, respectively; two tailed *t*-test). We concluded that the decreases in LFP, MUA and action potentials were roughly equivalent in their ability to predict the NBR.

Distances in V1

To determine whether the DiNA could be mediated by circuitry within area V1, we measured the distance along the cortical sheet between the site where DiNA were observed (that is, the position of the electrode) and the closest positively responding region (that is, closest PBR) in V1 (**Supplementary Fig. 4** online). The distance averaged over the data sets in which DiNA in spiking activity were observed was 7.15 ± 3.14 mm (mean ± s.d., **Fig. 8**). This mean distance and the even longer distances observed in specific sessions were longer than the horizontal connections in V1, which are 3–4 mm long (refs. 29,30). Thus, the horizontal connections cannot be the exclusive neuronal substrate mediating the decreases in neuronal activity that we observed (**Supplementary Discussion** online).

DISCUSSION

We have demonstrated that the occurrence of NBR in monkey striate cortex is associated with DiNA relative to spontaneous activity (**Fig. 2**). The variance in the time course of the NBR could be better accounted for by the local DiNA than by a model that assumed a purely vascular origin (**Fig. 5**). The BOLD signal is inversely proportional to the local content of deoxyhemoglobin (deoxy-Hb). Thus, in the NBR regions, the content of deoxy-Hb must have increased. A simple mechanism that could account for the increase in deoxy-Hb is a decrease in CBF that is larger in amplitude than the corresponding decreases in oxygen consumption. Indeed, such negative CBF responses have been reported in humans[16] and monkeys[31] using stimulation protocols similar to the one applied here. The measured decreases in CBF were found to be larger than the corresponding computed decreases in oxygen consumption[16]. The neurovascular mechanism underlying decreases in CBF could involve the constriction of arterioles regulated locally[32,33]. We conclude that, qualitatively, the amplitude relationship between

changes in neuronal activity, oxygen consumption, CBF and BOLD are symmetrical around the baseline.

Our data show, however, quantitative differences between the amplitudes of NBR and PBR relative to the corresponding changes in neuronal activity. The mean ratio of the NBR to DiNA was 1.63 times the corresponding ratio of PBR to increases in neuronal activity (**Supplementary Fig. 5** online; $P < 3.5 \times 10^{-4}$, two-tailed *t*-test). To a degree, the difference in ratios can be accounted for by the nonlinear relationship between the BOLD signal and CBF, and by the BOLD ceiling (saturation) effect[34–35]. The PBR and positive CBF response to the stimulus we used were larger than the corresponding NBR and negative CBF response. Thus, the positive response covers larger changes in CBF than the negative response, traversing more overall curvature in the relationship of BOLD to CBF (ref. 35). The expected result is a smaller amplitude of BOLD in the positive domain than in the negative domain for the same change in neuronal activity and CBF. Thus, a conservative estimate that assumes linearity suggests that more than 60% of the NBR can be accounted for by the DiNA.

Another factor contributing to the difference in ratios of NBR and PBR to decreases and increases in neuronal activity could be a component of NBR that is independent of the local changes in neuronal activity. Such a purely vascular component may explain the results of two of our experiments, in which low-amplitude NBRs were associated with low-amplitude increases rather than DiNA (**Fig. 2** and **Supplementary Fig. 2**). The notion of vascular contribution is also supported by the low amplitude, negative hemodynamic response measured optically in the rat, which do not correspond to any observable changes in neuronal activity[22]. The mechanism underlying vascular contributions may involve passively caused decreases in arterial CBF to the nonstimulated regions, stemming from a spatial redistribution of CBF caused by decrease in the resistance of dilated arterial vessels that supply the stimulated regions (ref. 16 and D.A. Boas, A. Devor, S.R. Jones, A.K. Dunn & A.M. Dale. *Soc. Neurosci. Abstr.* 454.2, 2005). Vascular contributions could be caused, in addition, by increases in deoxy-Hb in the venous compartment within the nonstimulated regions, elicited by venous back pressure; this back pressure could be induced by the downstream increase in venous blood pressure following the drainage of blood from the adjacent PBR regions and the resistance and limited compliance of the venous compartments[35] (D.A. Boas *et al.*, *Soc. Neurosci. Abstr.* 454.2, 2005).

No cardinal impulse response function can be estimated for the neurovascular system[7], and the relationship between the positive hemodynamic response and increases in neuronal activity cannot be automatically generalized for every condition or across brain regions[7,36]. Similarly, we suggest that the neuronal mechanisms underlying the NBR demonstrated here cannot be automatically generalized either. In particular, NBR and the increase in deoxy-Hb content could also be the result of increases in neuronal activity and oxygen consumption, accompanied by smaller increases or no increases at all in CBF (refs. 16,36). These mechanisms behind decreases in BOLD below baseline are likely to underlie the initial negative response ('initial dip') in stimulated regions[37–39]. They cannot, however, account for the NBRs demonstrated here, which were associated with decreases in neuronal activity. Moreover, the association of NBR with decreases in oxygen consumption, which has been shown in human visual cortex[16] using a protocol similar to that used here, has been confirmed and generalized to other protocols in the motor cortex[28] and visual cortex[40]. We do not necessarily expect NBR and/or DiNA in response to every task or in all brain areas. However, based on our findings in V1, together with the similarities in neurovascular regulation[41] and the structure of the vascular system[42] across the cerebral cortex, we do expect DiNA relative to baseline to be followed by NBR regardless of the experimental protocol or cortical region.

In the general case of encountering NBR with no available measurements of neuronal activity, the interpretation of NBR as reflecting decreases in neuronal activity could be inferred based on the following. NBR primarily in gray matter is likely to reflect DiNA, especially in primate cortex where no vascular shunts are known to exist[42]. In contrast, NBR primarily in large veins may reflect venous back pressure (D.A. Boas *et al.*, *Soc. Neurosci. Abstr.* 454.2, 2005). NBR with amplitude comparable to adjacent PBR or spatially isolated from PBR (ref. 26) could be interpreted as DiNA (ref. 25), as no PBR exists that could cause either passive decrease in CBF or back pressure. Low-amplitude NBR adjacent to PBR of substantially higher amplitude could reflect a vascular phenomenon as well as decreases in neuronal activity.

It is well established that different frequency ranges of the comprehensive broadband signal reflect different neural events at different neuronal sites[17,43]. Specifically, the LFP and MUA are good measures of input and local processing within a cortical area, and its spiking output, respectively. An examination of the spectrograms corresponding to the neuronal data presented here confirmed the findings previously reported for the PBR (ref. 7). Specifically, the LFP responses triggered by the overlapping stimuli had larger amplitudes than the corresponding increases in MUA and spiking activity (**Figs. 2** and **6**) and were better predictors of the PBR than were the MUA and action potential responses[7,13] (**Fig. 7**). The changes in spiking and field potentials during NBR were different from those observed for PBR. The decreases in action potentials in response to the nonoverlapping stimuli were larger than the corresponding decreases in LFP. In addition, the predictability of the NBR on the basis of LFP, MUA and action potentials was more balanced. Small differences in the predictability of the NBR based on the LFP and MUA might have been missed by our measurements, owing to the considerably smaller fractional changes of both NBR and DiNA as compared to those of the corresponding positive responses, and the reduced signal-to-noise ratio of the LFPs resulting from the transfer function of our acquisition system[7]. The NBR we demonstrated reflects changes in neuronal activity elicited by neuronal interactions rather than by direct sensory stimulation. The differences in the relationship of LFP and spiking activity to the PBR and NBR may reflect differences in the balance of excitation and inhibition between regions that receive direct stimulation and adjacent regions in which changes in activity are induced by neuromodulation originating in the stimulated regions. Alternatively, the differences we observed between the negative and positive responses in amplitude ratios and predictability could be accounted for by a possible saturation-type nonlinear relationship between the LFP input and the action potential output. A linear relationship between action potentials and LFP near the baseline and the saturation of the spiking activity in response to large input amplitudes are consistent with our observations, even for the case that the fMRI response depends on the LFP alone throughout their dynamic ranges.

A BOLD poststimulus overshoot followed the NBR and was approximately in phase with the poststimulus undershoot that followed the PBR. It has been suggested that the latter is caused by elevated cerebral blood volume and/or hematocrit that return(s) to baseline more slowly than CBF (refs. 44,45) or by a continued elevation of oxygen metabolism following the cessation of stimulus[46]. The poststimulus undershoot (**Fig. 1d**) is associated, however, with decreases in neuronal activity[7] (see also **Figs. 2** and **6**). Whereas these data do not rule out underlying mechanisms of increased cerebral blood volume and/or prolonged increases in oxygen consumption, they do indicate

that the poststimulus undershoot could be caused in part by decreases in CBF triggered by the poststimulus decreases in neuronal activity.

Similarly, although with inverse sign, the poststimulus BOLD overshoot that follows the NBR in the nonstimulated regions (**Fig. 1d**) is associated with increases in neuronal activity in the LFP, MUA and action potential domains (**Figs. 2** and **6**). The convolution of the neuronal response with the hemodynamic impulse response tracked this poststimulus overshoot with good fidelity (**Fig. 5**), suggesting that the latter could be caused in part by increases in CBF triggered by the poststimulus increases in neuronal activity. The fact that the changes in neuronal signal match the BOLD poststimulus overshoot with good fidelity, starting slightly below baseline, is yet more evidence for the correspondence of NBR to DiNA.

In conclusion, we have demonstrated a negative BOLD response associated with DiNA relative to spontaneous activity beyond the stimulated regions of monkey V1. The correlation between the NBR and the DiNA and the ability to predict the time course of one response based on that of the other provide evidence of a link between the two phenomena. Although the tight coupling we have demonstrated does not prove causation, it indicates that a substantial component of the NBR originates in the decreased neuronal activity that triggers a local reduction in cerebral blood flow.

METHODS

The procedures used for surgery, anesthesia and simultaneous fMRI and electrical recordings have been described in detail elsewhere[7,17,47]. These procedures are outlined briefly below, whereas new methodological aspects are described in detail. See also **Supplementary Methods** online.

Animals. We obtained 15 data sets from 7 healthy, anesthetized monkeys (*macaca mulatta*, 6–9 kg) in 12 sessions. The study was approved by the local authorities (Regierungspraesidium) and were in full compliance with the guidelines of the European Community for the care and use of laboratory animals.

Alignment of the stimuli presented to the two eyes. The aggregate minimum response field of the neurons in the vicinity of the electrode was mapped using the monocular presentation of a bar and a round patch of flickering radial checkers. This procedure was carried out before and once every hour during data acquisition. Whenever the difference in the centers of the monocular receptive fields exceeded 1°, we shifted the stimulus presented to the right eye to achieve complete registration.

Visual stimulation. Ring stimuli centered on the center of the visual field and composed of high-contrast radial checkers rotating at 60° per s were presented to the monkeys. The stimulated eccentricities (in the range of 1.5°–15°) were adjusted such that one stimulus overlapped the receptive field whereas the other did not. The eccentricities spanned by each of the rings were determined according to the retinotopic map[47] such that the expected width of the activated cortical strip in V1 was in the range of 10–15 mm. The background was a uniform gray field with luminance equal to the mean luminance of the checkers. The same luminance was used in the blank gray image presented during the control periods.

Each scan started with a 40-s control period followed by eight epochs of 20 s stimulus-on and 25 s stimulus-off. The nonoverlapping stimulus was presented in three times as many epochs as the overlapping stimulus. The order in which the two stimuli were presented was systematically varied, such that all possible combinations fulfilling the above-mentioned 3:1 ratio were sampled equally.

fMRI data analysis and selection of voxels. Voxel-wise cross-correlation analysis[48] was applied, using templates of the stimulation protocol convolved with a model of the hemodynamic response[49]. A threshold was applied to the cross-correlation images, followed by a minimal spatial cluster operator of at least four significantly responding voxels. The clustering was measured in two dimensions, with any of the eight immediate neighbors of a pixel defined as contiguous. The minimal cluster operator was applied separately for the NBR and the PBR. Voxel-wise cross-correlation *p*-values were corrected for multiple comparisons according to the cluster size threshold[50]. The fMRI signal was sampled and averaged over the voxels within the ROI around the electrode (mean volume across sessions: $7.0 \times 2.3 \times 6.0 \pm 3.1$ mm^3). The sampling and averaging was limited to voxels in which the response (either to direct stimulation of the region of the electrode or to stimulation away from that region) passed the cross-correlation threshold and clustering operator. The amplitude of the fMRI response was computed by averaging the response over the 12 s starting 2 s after the onset of the stimulus. The starting point of the averaging (2 s) was selected to take into account the delay in the onset of the hemodynamic response. The length of time over which we averaged (12 s) was chosen to fit the period before both the NBR and the decreases in neural activity adapted to an amplitude smaller than the peak amplitude. These two parameters were determined based on the time course averaged over all data sets and were kept fixed for the analysis of all data sets.

Electrophysiological data analysis. Neuronal activity was measured by digitizing the broadband electrophysiological signal. Offline elimination of residual gradient interference[7] was applied. Two types of signals were extracted from the broadband de-noised neuronal signal. First, to obtain the comprehensive neuronal signal, we applied Fourier decomposition separately to nonoverlapping 1-s portions of the broadband de-noised electrophysiological signal. (Note that 1 s was also the acquisition time of one MR volume.) The resulting spectrogram showed power as a function of frequency and time in successive 1 s epochs. The global neuronal activity was estimated by averaging the fractional change in power over the whole range of frequencies (4–3,000 Hz). The LFP and MUA were estimated by averaging the fractional change in power over the ranges of 30–130 Hz and 300–2,500 Hz, respectively. Second, by matching a template of action potential to the de-noised signal, we identified spikes that were estimated to originate from neurons in the close vicinity (that is, within approximately 50 μm) of the electrode. The amplitude of the neuronal response was computed by averaging the time course over the 12 s starting with the onset of the stimulus.

Trial-by-trial BOLD/neuronal correlation analysis. We first computed the trial-by-trial fluctuations in the BOLD response in one session around the mean BOLD response. To this end, we used linear regression: the mean second-to-second time course of the BOLD response was the explanatory variable, and the second-to-second time course within each trial was the dependent variable. The trial-by-trial computed slopes of the regression were used as the amplitude of the BOLD response. A similar analysis was applied to compute the trial-by-trial amplitudes of the comprehensive neuronal response (**Fig. 4**). The time course over the entire period of the trial was considered (5 s baseline, 20 s stimulation, 20 s poststimulation, for a total of 45 s), both in the positive and negative domains (**Fig. 4**). This analysis was repeated while considering only the periods of prestimulus baseline and stimulation (that is, excluding post-stimulation data; **Supplementary Fig. 3** online). The starting point of the considered time course of the BOLD response was delayed by 2 s compared to the starting point of the neuronal response, in order to take into account the delay of the hemodynamic response. To remove slow changes in BOLD and neuronal response over the course of any particular session, each of the vectors of trial-by-trial amplitudes was high-pass filtered (the convolution of the vector with a Gaussian (s.d. = 10 trials) was subtracted from the vector). The vectors of trial-by-trial amplitudes of BOLD and neuronal responses were then used for the correlation analysis (**Fig. 4**).

Trial-by-trial prediction of BOLD response based on LFP, MUA and action potentials. To compute the trial-by-trial predicted positive or negative BOLD response (**Fig. 7**), the corresponding LFP, MUA or action potential response was convolved with the impulse response (**Fig. 5j**). The trial-by-trial correlation coefficient between the second-to-second predicted time course of BOLD response and the second-to-second measured time course of BOLD response (**Fig. 7**) was then computed. The time course over the entire period of the trial was considered, both in the positive and negative domains.

Note: Supplementary information is available on the Nature Neuroscience website.

ACKNOWLEDGMENTS

We thank A. Bartels, A. Ghazanfar, K. Hoffman, A. Ishai, C. Kayser, G. Rainer, S. Smirnakis, L. Sugrue and K. Uludag for comments on a previous version of the manuscript; D. Blaurock for English editing; and S. Weber for fine-mechanic work. This study was supported by a long-term fellowship from the European Molecular Biology Organization awarded to A.S., and by the Max Planck Society.

AUTHOR CONTRIBUTIONS

A.S. designed the study, carried out the experiments together with M.A., wrote the analysis software, analyzed the data and wrote the manuscript. M.A. carried out the experiments together with A.S. A.O. designed the hardware for gradient interference compensation. N.K.L. wrote the software for removing residual interference from the electrical signal and for analysis of the neuronal signal, and supervised the study.

COMPETING INTERESTS STATEMENT

The authors declare that they have no competing financial interests.

Published online at http://www.nature.com/natureneuroscience
Reprints and permissions information is available online at http://npg.nature.com/reprintsandpermissions/

1. Raichle, M.E., Martin, W.R.W., Herscovitch, P., Mintun, M.A. & Markham, J. Brain blood-flow measured with intravenous H2(15)O. II. Implementation and validation. *J. Nucl. Med.* **24**, 790–798 (1983).
2. Ogawa, S., Lee, T.M., Kay, A.R. & Tank, D.W. Brain magnetic resonance imaging with contrast dependent on blood oxygenation. *Proc. Natl. Acad. Sci. USA* **87**, 9868–9872 (1990).
3. Kwong, K.K. *et al.* Dynamic magnetic resonance imaging of human brain activity during primary sensory stimulation. *Proc. Natl. Acad. Sci. USA* **89**, 5675–5679 (1992).
4. Ogawa, S. *et al.* Intrinsic signal changes accompanying sensory stimulation: functional brain mapping with magnetic-resonance-imaging. *Proc. Natl. Acad. Sci. USA* **89**, 5951–5955 (1992).
5. Bandettini, P.A., Wong, E.C., Hinks, R.S., Tikofsky, R.S. & Hyde, J.S. Time course EPI of human brain function during task activation. *Magn. Reson. Med.* **25**, 390–397 (1992).
6. Mathiesen, C., Caesar, K., Akgoren, N. & Lauritzen, M. Modification of activity-dependent increases of cerebral blood flow by excitatory synaptic activity and spikes in rat cerebellar cortex. *J. Physiol. (Lond.)* **512**, 555–566 (1998).
7. Logothetis, N.K., Pauls, J., Augath, M., Trinath, T. & Oeltermann, A. Neurophysiological investigation of the basis of the fMRI signal. *Nature* **412**, 150–157 (2001).
8. Smith, A.J. *et al.* Cerebral energetics and spiking frequency: the neurophysiological basis of fMRI. *Proc. Natl. Acad. Sci. USA* **99**, 10765–10770 (2002).
9. Sheth, S. *et al.* Evaluation of coupling between optical intrinsic signals and neuronal activity in rat somatosensory cortex. *Neuroimage* **19**, 884–894 (2003).
10. Thompson, J.K., Peterson, M.R. & Freeman, R.D. Single-neuron activity and tissue oxygenation in the cerebral cortex. *Science* **299**, 1070–1072 (2003).
11. Devor, A. *et al.* Coupling of total hemoglobin concentration, oxygenation, and neural activity in rat somatosensory cortex. *Neuron* **39**, 353–359 (2003).
12. Kayser, C., Kim, M., Ugurbil, K., Kim, D.S. & Konig, P. A comparison of hemodynamic and neural responses in cat visual cortex using complex stimuli. *Cereb. Cortex* **14**, 881–891 (2004).
13. Niessing, J. *et al.* Hemodynamic signals correlate tightly with synchronized gamma oscillations. *Science* **309**, 948–951 (2005).
14. Mukamel, R. *et al.* Coupling between neuronal firing, field potentials, and fMR1 in human auditory cortex. *Science* **309**, 951–954 (2005).
15. Shulman, G.L. *et al.* Common blood flow changes across visual tasks: II. Decreases in cerebral cortex. *J. Cogn. Neurosci.* **9**, 648–663 (1997).
16. Shmuel, A. *et al.* Sustained negative BOLD, blood flow and oxygen consumption response and its coupling to the positive response in the human brain. *Neuron* **36**, 1195–1210 (2002).
17. Logothetis, N.K. The neural basis of the blood-oxygen-level-dependent functional magnetic resonance imaging signal. *Phil. Trans. R. Soc. Lond. B* **357**, 1003–1037 (2002).
18. Tootell, R.B.H. *et al.* The retinotopy of visual spatial attention. *Neuron* **21**, 1409–1422 (1998).
19. Saad, Z.S., Ropella, K.M., Cox, R.W. & Deyoe, E.A. Analysis and use of fMRI response delays. *Hum. Brain Mapp.* **13**, 74–93 (2001).
20. Harel, N., Lee, S.P., Nagaoka, T., Kim, D.S. & Kim, S.G. Origin of negative blood oxygenation level-dependent fMRI signals. *J. Cereb. Blood Flow Metab.* **22**, 908–917 (2002).
21. Kannurpatti, S.S. & Biswal, B.B. Negative functional response to sensory stimulation and its origins. *J. Cereb. Blood Flow Metab.* **24**, 703–712 (2004).
22. Devor, A. *et al.* Coupling of the cortical hemodynamic response to cortical and thalamic neuronal activity. *Proc. Natl. Acad. Sci. USA* **102**, 3822–3827 (2005).
23. Allison, J.D., Meader, K.J., Loring, D.W., Figueroa, R.E. & Wright, J.C. Functional MRI cerebral activation and deactivation during finger movement. *Neurology* **54**, 135–142 (2000).
24. Raichle, M.E. *et al.* A default mode of brain function. *Proc. Natl. Acad. Sci. USA* **98**, 676–682 (2001).
25. Gusnard, D.A. & Raichle, M.E. Searching for a baseline: functional imaging and the resting human brain. *Nat. Rev. Neurosci.* **2**, 685–694 (2001).
26. Smith, A.T., Williams, A.L. & Singh, K.D. Negative BOLD in the visual cortex: evidence against blood stealing. *Hum. Brain Mapp.* **21**, 213–220 (2004).
27. Gold, L. & Lauritzen, M. Neuronal deactivation explains decreased cerebellar blood flow in response to focal cerebral ischemia or suppressed neocortical function. *Proc. Natl. Acad. Sci. USA* **99**, 7699–7704 (2002).
28. Stefanovic, B., Warnking, J.M. & Pike, G.B. Hemodynamic and metabolic responses to neuronal inhibition. *Neuroimage* **22**, 771–778 (2004).
29. Gilbert, C.D. & Wiesel, T.N. Morphology and intra-cortical projections of functionally characterized neurons in the cat visual cortex. *Nature* **280**, 120–125 (1979).
30. Rockland, K.S. & Lund, J.S. Intrinsic laminar lattice connections in primate visual cortex. *J. Comp. Neurol.* **216**, 303–318 (1983).
31. Pfeuffer, J., Merkle, H., Beyerlein, M., Steudel, T. & Logothetis, N.K. Anatomical and functional MR imaging in the macaque monkey using a vertical large-bore 7 Tesla setup. *Magn. Reson. Imaging* **22**, 1343–1359 (2004).
32. Mulligan, S.J. & MacVicar, B.A. Calcium transients in astrocyte endfeet cause cerebrovascular constrictions. *Nature* **431**, 195–199 (2004).
33. Cauli, B. *et al.* Cortical GABA interneurons in neurovascular coupling: relays for subcortical vasoactive pathways. *J. Neurosci.* **24**, 8940–8949 (2004).
34. Hoge, R.D. *et al.* Investigation of BOLD signal dependence on cerebral blood flow and oxygen consumption: the deoxyhemoglobin dilution model. *Magn. Reson. Med.* **42**, 849–863 (1999).
35. Buxton, R.B., Uludag, K., Dubowitz, D.J. & Liu, T.T. Modeling the hemodynamic response to brain activation. *Neuroimage* **23**, S220–S233 (2004).
36. Lauritzen, M. Reading vascular changes in brain imaging: is dendritic calcium the key? *Nat. Rev. Neurosci.* **6**, 77–85 (2005).
37. Malonek, D. & Grinvald, A. Interactions between electrical activity and cortical microcirculation revealed by imaging spectroscopy: implications for functional brain mapping. *Science* **272**, 551–554 (1996).
38. Menon, R.S. *et al.* Bold based functional MRI at 4-tesla includes a capillary bed contribution: echo-planar imaging correlates with previous optical imaging using intrinsic signals. *Magn. Reson. Med.* **33**, 453–459 (1995).
39. Logothetis, N.K., Guggenberger, H., Peled, S. & Pauls, J. Functional imaging of the monkey brain. *Nat. Neurosci.* **2**, 555–562 (1999).
40. Uludag, K. *et al.* Coupling of cerebral blood flow and oxygen consumption during physiological activation and deactivation measured with fMRI. *Neuroimage* **23**, 148–155 (2004).
41. Iadecola, C. Neurovascular regulation in the normal brain and in Alzheimer's disease. *Nat. Rev. Neurosci.* **5**, 347–360 (2004).
42. Duvernoy, H.M., Delon, S. & Vannson, J.L. Cortical blood vessels of the human-brain. *Brain Res. Bull.* **7**, 519–579 (1981).
43. Logothetis, N.K. The underpinnings of the BOLD functional magnetic resonance imaging signal. *J. Neurosci.* **23**, 3963–3971 (2003).
44. Mandeville, J.B. *et al.* Dynamic functional imaging of relative cerebral blood volume during rat forepaw stimulation. *Magn. Reson. Med.* **39**, 615–624 (1998).
45. Buxton, R.B., Wong, E.C. & Frank, L.R. Dynamics of blood flow and oxygenation changes during brain activation: the balloon model. *Magn. Reson. Med.* **39**, 855–864 (1998).
46. Lu, H., Golay, X., Pekar, J.J. & van Zijl, P.C.M. Sustained poststimulus elevation in cerebral oxygen utilization after vascular recovery. *J. Cereb. Blood Flow Metab.* **24**, 764–770 (2004).
47. Brewer, A.A., Press, W.A., Logothetis, N.K. & Wandell, B.A. Visual areas in macaque cortex measured using functional magnetic resonance imaging. *J. Neurosci.* **22**, 10416–10426 (2002).
48. Bandettini, P.A., Jesmanowicz, A., Wong, E.C. & Hyde, J.S. Processing strategies for time-course data sets in functional MRI of the human brain. *Magn. Reson. Med.* **30**, 161–173 (1993).
49. Boynton, G.M., Engel, S.A., Glover, G.H. & Heeger, D.J. Linear systems analysis of functional magnetic resonance imaging in human V1. *J. Neurosci.* **16**, 4207–4221 (1996).
50. Forman, S.D. *et al.* Improved assessment of significant activation in functional magnetic resonance imaging (fMRI): use of a cluster-size threshold. *Magn. Reson. Med.* **33**, 636–647 (1995).